Hindawi
Advances in Materials Science and Engineering
Volume 2021, Article ID 5548638, 12 pages
https://doi.org/10.1155/2021/5548638

Research Article

A New Mitigation Measure to Counter Thermal Instability of Air-Cooled Embankment in Sandy Permafrost Zones of Tibet Plateau

Minghao Liu, Jing Luo, Liang Zhang, and Xin Ju

State Key Laboratory of Frozen Soil Engineering, Northwest Institute of Eco-Environment and Resources, Chinese Academy of Sciences, Lanzhou 730000, Gansu, China

Correspondence should be addressed to Minghao Liu; liuminghao@lzb.ac.cn

Received 2 February 2021; Revised 13 February 2021; Accepted 24 March 2021; Published 8 April 2021

Academic Editor: Robert Cerný

A crushed-rock revetment (CRR) with high permeability that can be paved on embankment slopes is widely used to cool and protect the subgrade permafrost. In this study, a traditional CRR over warm permafrost was selected to investigate its cooling characteristics based on the ground temperature observed from 2003 to 2014. A new mitigation structure (NMS) was designed to improve the cooling capacity of the CRR and to counter the pore-filling of the rock layer. Numerical simulations were conducted to evaluate the cooling performance and reinforcing capacity of the NMS based on a developed heat and mass transfer model. The results indicate that the traditional CRR can improve the symmetry of the permafrost subgrade and decrease the ground temperature of shallow permafrost. However, the CRR cannot generate strong enough cooling to influence the deep (below 10 m depth) and warm permafrost with a mean annual ground temperature above −1.0°C. The wind-blown sand can further weaken the cooling of the CRR and cause significant permafrost warming and thawing beneath the slopes, posing a severe threat to the long-term safe operation of the embankment. The proposed NMS can produce a significantly superior cooling performance to the CRR. If the CRR is reinforced by the new structure, it can not only effectively cool the underlying warm permafrost but also elevate the permafrost table. The new structure can also protect the rock layer on the slopes from sand-filling. The NMS can be used as an effective method for roadbed design or maintenance over warm permafrost.

1. Introduction

Permafrost is soil or rock with ice that remains at or below 0°C for at least two consecutive years [1, 2]. Land in permafrost zones is permanently frozen to a great depth, with the surface seasonally thawing in the summer [1, 2]. Approximately, 25% of the land area in the Northern Hemisphere is underlain by permafrost stratum [3], which is, however, a type of unstable geological body and highly sensitive to ground temperature changes due to the existence of ground ice [4, 5]. Many critical transportation infrastructures were constructed in the permafrost zones, including the East-Siberian Railway in Russia, the Hudson Bay Railway in Canada, the Alaska Highway in the USA, and the Qinghai-Tibet Railway and Highway in China [6]. Roadway construction in permafrost zones generally disturbs the original ground surface and changes the ground-surface energy balance, leading to the warming and melting of the ice-rich permafrost underneath the embankment and the subsequent uneven thaw settlement [7, 8]. This severely affects the stability and integrity of transportation infrastructures and threatens their long-term safe operation [9]. How to control the ground heat to meet the demand of engineering foundation thermal stability is an important issue in permafrost areas.

The Qinghai-Tibet Plateau (QTP), with an average elevation of over 4000 m, is one of the highest plateaus in the world and contains the largest area of permafrost at high elevation on Earth [10]. Permafrost on the QTP is typically warmer compared with other areas of the northern hemisphere [10, 11] and thus more susceptible to temperature perturbation. Climate warming on the QTP can accelerate

permafrost warming and has caused permafrost degradation in recent decades [6, 12]. This leads to the decrease of bearing-capacity of the permafrost foundation and potentially causes the large settlements or failures of the transportations traversed the permafrost areas of the QTP, for example, Qinghai-Tibet Railway, the Qinghai-Tibet Highway, Gongyu Expressway, and so on. Mitigation techniques have been developed based on the active cooling approach to cool the subgrade foundation and to protect the underlying permafrost foundation on the QTP in recent decades [6]. The crushed-rock embankment is a type of air convection embankment by making the best use of cold air energy during cold seasons and has been widely employed in roadbed engineering over permafrost on the QTP [13]. The crushed-rock embankment is constructed using poorly graded rocks with high permeability that can allow air to flow through the rock pores and augment heat extraction from the embankment during winter [12, 14]. It has proven to be an economical and effective technique to cool the permafrost stratum and maintain the foundation stability of embankments [12, 15].

Crushed-rock revetment (CRR), paving the rocks on the side slopes, is one of the typical construction methods of air convection embankment [6, 16]. Although the CRR is prevalent in practical engineering because of its convenient construction and flexible reinforcement, it is facing problems that affect its long-term effective cooling performances. It is particularly concerning that the CRR generates insufficient cooling on the underlying warm permafrost with a mean annual ground temperature above −1.0°C [17, 18]. The limited cooling largely lies in the hot wind that blows into the pore space of the open crushed-rock layer in hot seasons, which can increase heat absorption in the embankment slopes, and is adverse to permafrost stability. The aeolian sands and wreathed rocks frequently occurred on the QTP due to the strong wind and high ultraviolet radiation [19, 20], as is shown in Figure 1, which can block the pore of the rocks and further reduce its convection cooling capacity, aggravating the long-term performance of the CRR. How to optimize it to enhance its cooling performance to counter permafrost degradation and climate warming has become an urgent issue in complex circumstances.

In this study, we firstly investigated the cooling characteristics of a selected CRR embankment in a warm permafrost zone based on the ground temperature observed from 2004 to 2014. Then, a mitigation structure was designed to improve the cooling capacity of the CRR and to counter the sand-filling of the porous rock layer. A coupled heat transfer model was developed and series of numerical simulations were conducted to evaluate the cooling effect and reinforcing performance of the new structure considering climate warming. It is hoped that this study could improve the utilization of cold energy in cold regions and provide guidance for the design and maintenance of embankment traversed warm or thaw-sensitive permafrost zones.

2. Field Observations and Analysis

2.1. Slow Permafrost Warming under the CRR Embankment. As shown in Figure 2, a CRR embankment built in Chuma'er High Plain along the Qinghai-Tibet Railway was selected to analyze its long-term cooling effect and characteristic, based on the observed ground temperature data from 2003 to 2014. Permafrost in this site is typically warm and ice-rich, with a mean annual ground temperature of about −0.9°C. The permafrost table ranges from 2.5 m to 3.0 m. Thus, this region of the monitoring section located is representative of the warm and ice-rich permafrost of the QTP. The thickness of the crushed-rock layer on the sunny and shady slopes of the embankments is 1.6 m and 0.8 m, respectively. Four boreholes with a depth of 16 m were drilled at the two shoulders and the two slope toes of the railway embankment, and one borehole with a depth of 16 m was also drilled in the undisturbed ground as a reference of permafrost thermal status without disturbance, which is 10 m away from the embankment toe. The ground temperatures were measured by thermistors cable with a precision of ±0.02°C, installed in the embankment boreholes. The data was collected manually by a CR3000 data logger two times a month.

Figure 3 shows the ground temperature fields of the CRR embankment in early October of the years 2003, 2005, 2010, and 2014. The 0°C isotherm in the figure is defined as the permafrost table because the maximum seasonal thaw depth usually occurs in October on the QTP. As shown, the permafrost table under the sunny side (left side) of the embankment was slightly deeper than the shady side (right side) and the natural ground in 2003 after the embankment was just constructed. This was mainly due to thermal disturbance caused by embankment construction, while, in 2005, the permafrost table beneath the embankment was elevated obviously, with a magnitude of approximately 2.0 m, revealing the cooling effect of the CRR on the underlying permafrost. Up to 2010, the cooling for the permafrost layer with a depth of −3.0 to −5.0 m continued, which can be confirmed by the elevation of the −0.5°C isotherm under the embankment. The symmetry of the ground temperature field was also improved although the embankment orientation is southeast-northwest direction, which tends to cause different solar radiation on the sunny slope and shady slope of the embankment [21]. It proved that different thickness of the CRR on the two slopes performed satisfactory effects in improving the symmetry of the ground temperature distribution. In 2014, the symmetrical temperature field was maintained and the permafrost table under the embankment was further elevated. These characteristics revealed the good cooling of this structure on the shallow permafrost. However, it should be noted that the deep permafrost experienced a slow warming trend since constructed, as shown by the disappearance of the −1.0°C isotherm.

For further investigation of dynamic variation of permafrost temperatures, Figure 4 was drawn to show time series of permafrost temperatures with depths of 2.0 m, 4.0 m, and 10 m beneath the sunny shoulder of the CRR embankment. The depths were measured from the original ground surface, which represented the shallow and deep permafrost. It can be clearly found that permafrost at the depths of 2.0 m and 4.0 m experienced obvious cooling processes after construction. Particularly after 2008, the temperature amplitude increased, indicating that the heat exchange process during cold seasons increased. In the contrary, the deep permafrost temperature at depth of 11 m

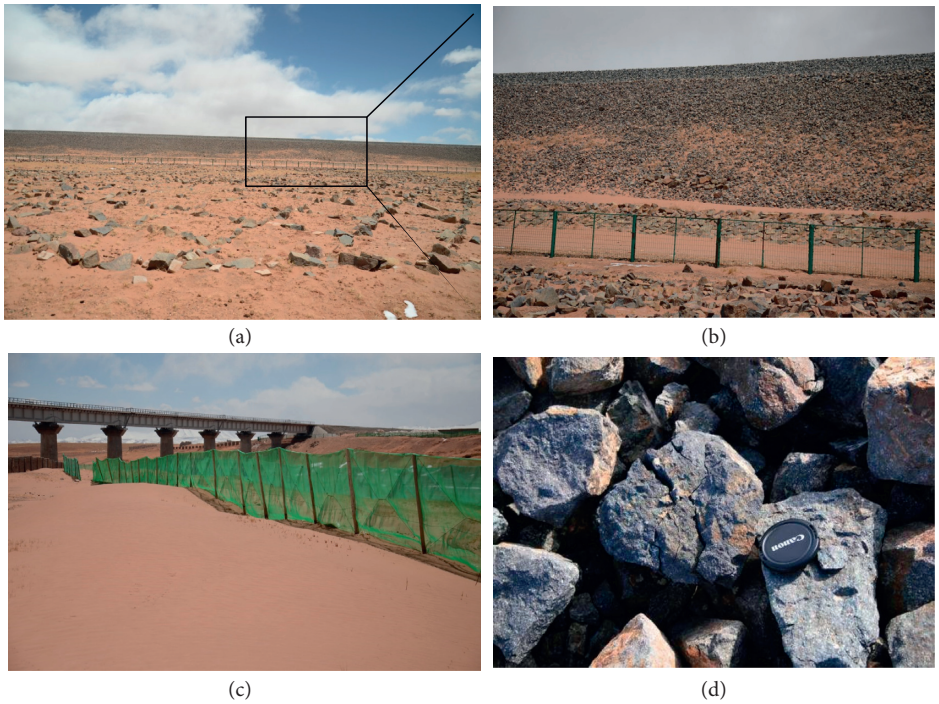

Figure 1: Wind-blown sand and rock-weathering of CRR embankment along the Qinghai-Tibet Railway. (a) Sand-filling of porous rock layer at the Honglianghe section; (b) close-view of sand-filling of the CRR; (c) prevalent sand prevention measure on the QTP; and (d) rock-weathering of the CRR caused by a severe environment.

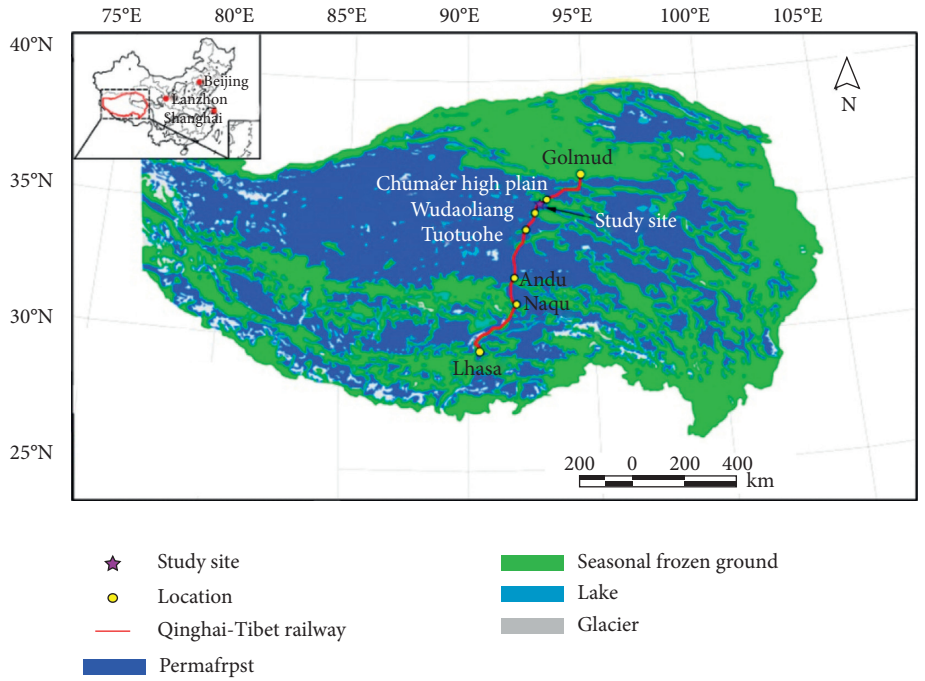

Figure 2: Location of the monitored CRR embankment in the permafrost zone of the QTP. Permafrost data were from the China cold and arid scientific data center (http://westdc.westgis.ac.cn/).

under CRR embankment was rising slowly, with an increase of nearly 0.22°C from 2003 to 2014. Although the warming rate decreased after 2008, the warming trend continued. Thus, it is concluded that the cooling effect of the CRR was relatively limited and could not effectively cool the deeper permafrost.

The long-term monitoring results revealed that the deep permafrost beneath the CRR experienced a significant warming

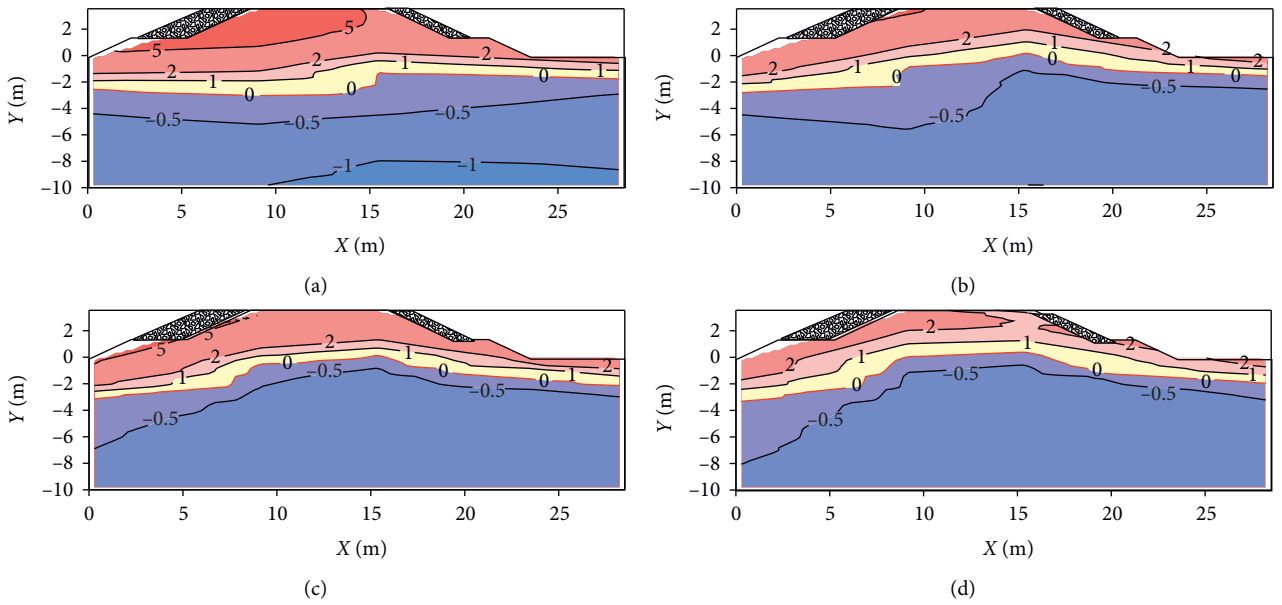

Figure 3: Temperature fields of the monitored CRR embankment on October 1 each year. (a) 2003; (b) 2005; (c) 2010; and (d) 2014.

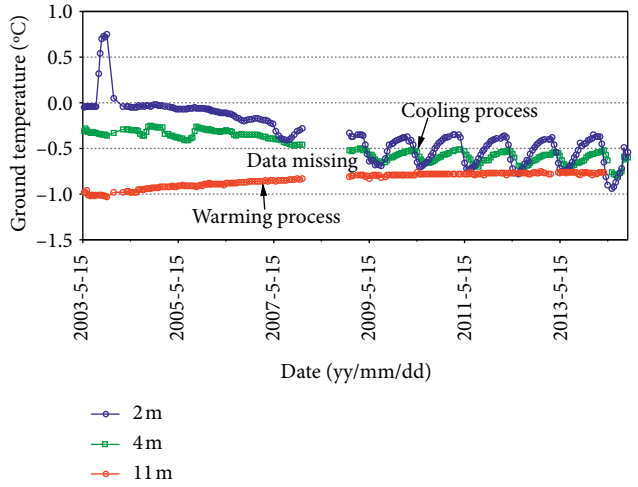

Figure 4: Variations of ground temperatures at depths of 2.0 m, 4.0 m, and 11.0 m beneath the monitored CRR embankment.

process, although the permafrost table beneath the embankment was elevated and the shallow grounds were cooled. The considerable warming of deep permafrost might generate compression deformation, which will reduce the embankment stability and potentially threaten the safe operation [22, 23]. The insufficient and unsatisfied cooling will be challenging the existing CRR to counteract the impact of climate warming in the warm or thaw-sensitive permafrost regions. Thus, how to optimize this structure and propose a new countermeasure is urgent to maintain the long-term thermal stability of embankment over warm permafrost on the QTP.

3. Numerical Modeling

3.1. The New Structure. In this section, a new mitigation measure (NMS) combined a CRR and a slope-warming prevention measure was designed as a countermeasure to improve the cooling capacity and to prevent wind-blown sand. As shown in Figure 5, a soil layer with geotextile was designed to pave on the CRR of the embankment slopes, which aims to prevent the warm wind from entering the rock layer during summer, to remove the solar radiation, and to strengthen convective heat transfer in rock layer during winter. A coupled heat transfer model was developed to evaluate the cooling effects and reinforcing performances of the new structure. Based on the heat and mass transfer theories, the air convection heat transfer in the porous layer and heat conduction with a phase transaction in the soil layers were considered in the model. The heat radiation of the rock layer was not considered in the model. Three sets of simulations were conducted to investigate the geothermal regimes evolution in different scenarios, as shown in Table 1. The geometrical model of

the three associated embankments (Figure 6) were referred to the embankment in the Tuotuohe section of the Qinghai-Tibet Railway where the sand-filing damage is widespread.

3.2. Governing Equations

3.2.1. Airflow outside the Porous Rock Layer. The airflow is considered as a turbulent flow at the atmosphere [24]. The air is assumed to be an incompressible fluid with constant physical properties, and the influence of the air temperature on the airflow velocity is negligible. We have the following governing equations for the airflow's turbulent heat transfer process [25]:

Continuity:

$$\frac{\partial v_x}{\partial x} + \frac{\partial v_y}{\partial y} = 0. \tag{1}$$

Momentum:

$$\rho\frac{\partial v_x}{\partial t} + \rho\left(\frac{\partial(v_x v_x)}{\partial x} + \frac{\partial(v_y v_x)}{\partial y}\right) = -\frac{\partial p}{\partial x} + \mu\left(\frac{\partial^2 v_x}{\partial x^2} + \frac{\partial^2 v_x}{\partial y^2}\right),$$

$$\rho\frac{\partial v_y}{\partial t} + \rho\left(\frac{\partial(v_x v_y)}{\partial x} + \frac{\partial(v_y v_y)}{\partial y}\right) = -\frac{\partial p}{\partial y} + \mu\left(\frac{\partial^2 v_y}{\partial x^2} + \frac{\partial^2 v_y}{\partial y^2}\right) - \rho_a g. \tag{2}$$

Energy:

$$\rho_a C_a\frac{\partial T}{\partial t} = \frac{\partial}{\partial x}\left(\lambda_a\frac{\partial T}{\partial x}\right) + \frac{\partial}{\partial y}\left(\lambda_a\frac{\partial T}{\partial y}\right) - \rho_a C_a\left(\frac{\partial(v_x T)}{\partial x} + \frac{\partial(v_y T)}{\partial y}\right), \tag{3}$$

where v_x and v_y are air speed along x- and y-axis; ρ_a is air density; p is air pressure; μ_a is dynamic viscosity, λ_a is air thermal conductivity, and C_a is air specific heat capacity.

3.2.2. Convective Heat Transfer in the Porous Rock Layer. The CRR was considered to be a porous medium in the model. Convection heat transfer of air in the porous layer is a heat and mass transfer process, and it is assumed that only the lacunal air movement is taken into consideration. The governing equations can be expressed as follows [16, 26]:

Continuity:

$$\frac{\partial v_x}{\partial x} + \frac{\partial v_y}{\partial y} = 0. \tag{4}$$

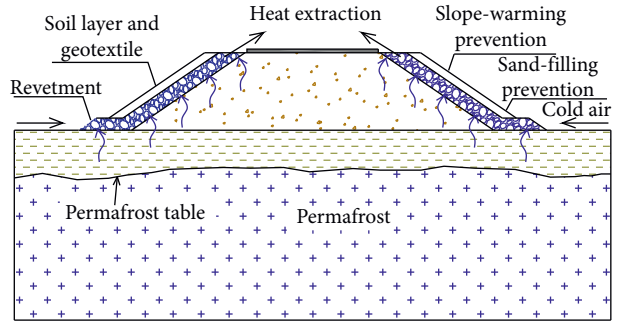

Figure 5: Schematic of the cooling of the proposed NMS.

Momentum:

$$\frac{\partial p}{\partial x} = -\frac{\mu}{k}v_x - \rho_a B|v|v_x,$$
$$\frac{\partial p}{\partial y} = -\frac{\mu}{k}v_y - \rho_a B|v|v_y - \rho_\alpha g. \tag{5}$$

Energy:

$$C^e\frac{\partial x}{\partial t} = \frac{\partial}{\partial x}\left(\lambda^e\frac{\partial T}{\partial x}\right) + \frac{\partial}{\partial y}\left(\lambda^e\frac{\partial T}{\partial y}\right) - \rho_a c_a\frac{\partial}{\partial x}\left(\frac{\partial(v_x T)}{\partial x} + \frac{\partial(v_y T)}{\partial y}\right), \tag{6}$$

where $|v| = \sqrt{v_x^2 + v_y^2}$, B is the inertial drag coefficient, k is the permeability of the porous medium, and Ce and λe are the effective volumetric heat capacity and effective thermal conductivity, respectively.

Air density $\rho\alpha$ can be expressed as a function of the temperature T and the Boussinesq approximation is used to simplify the computation:

$$\rho_\alpha = \rho[1 - \beta(T - T_0)], \tag{7}$$

where T_0 is the corresponding temperature of ρ and β is the thermal expansion coefficient of air.

3.2.3. Conductive Heat Transfer for Soil Layers and Embankment Filling. For soil layers and embankment fillings, the heat transfer process was dominated by the heat conduction, and the phase change process of ice to water needs to be considered when the freeze-thaw processes occur. The heat transfer process can be described as follows [25, 26]:

$$C^e\frac{\partial x}{\partial t} = \frac{\partial}{\partial x}\left(\lambda^e\frac{\partial T}{\partial x}\right) + \frac{\partial}{\partial y}\left(\lambda^e\frac{\partial T}{\partial y}\right). \tag{8}$$

We assume that the phase change of the media occurs in a range of temperatures ($T_p \pm \Delta T$). Based on the sensible heat capacity method [27], C^e and λ^e can be calculated as follows:

Table 1: Description of the designed scenarios with associated cases.

Cases	Designed scenarios description
Case 1	Embankment with the CRR performs a service life of 30 years
Case 2	Embankment with CRR performs for 10 years and then suffers from sand-filling for 20 years
Case 3	Embankment with CRR performs for 10 years and then reinforced with the NMS for 20 years

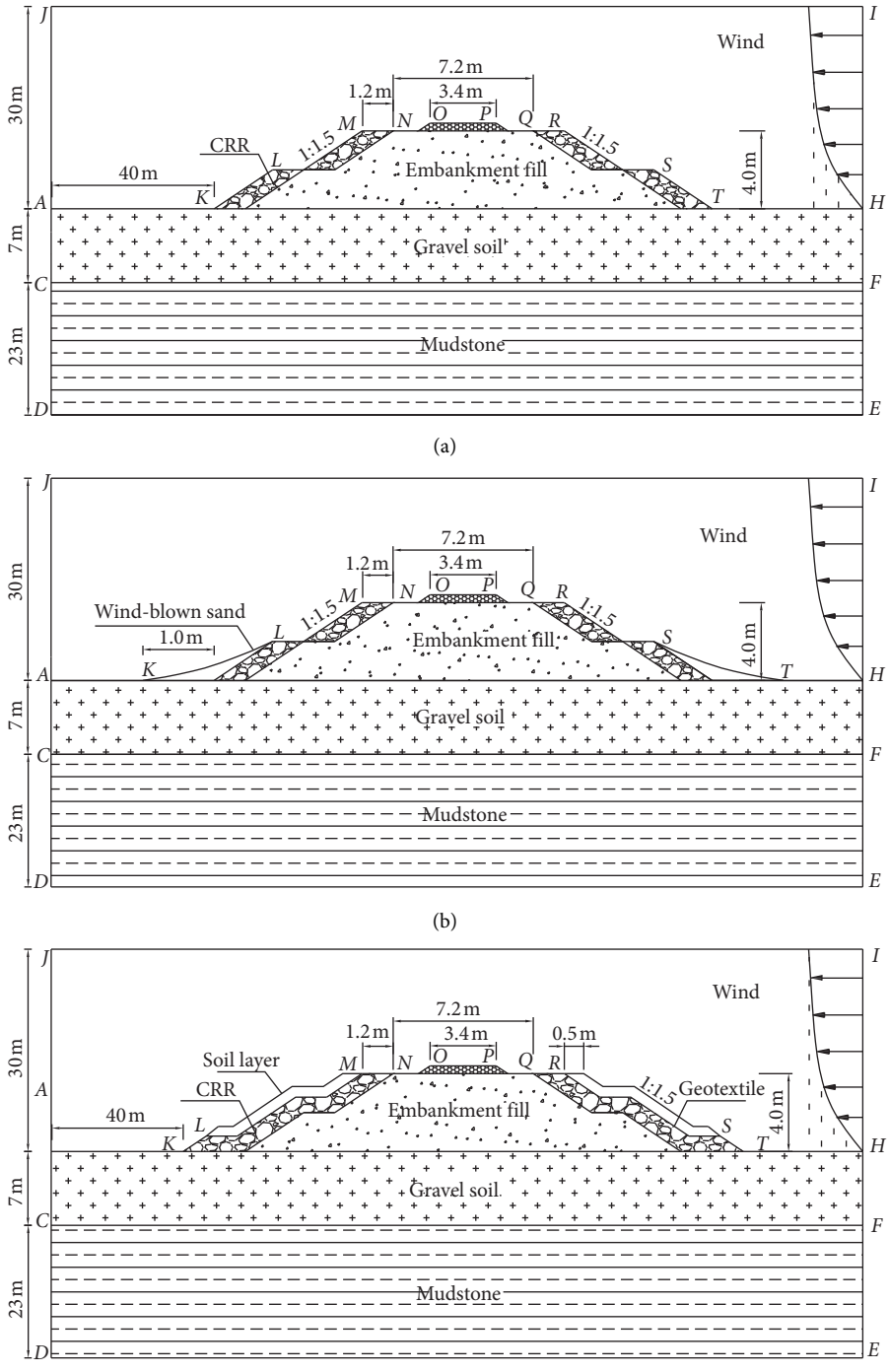

Figure 6: Geometrical model of the three associated embankments in three cases. (a) Case 1; (b) Case 2; and (c) Case 3.

$$C^e = \begin{cases} C_f, & T < (T_p - \Delta T), \\ \dfrac{l}{2\Delta T} + \dfrac{C_f + C_u}{2}, & (T_p - \Delta T) \le T \le (T_p + \Delta T), \lambda^e \\ C_u, & T > (T_p + \Delta T), \end{cases}$$
$$= \begin{cases} \lambda_f, & T < (T_p - \Delta T), \\ \lambda_f + \dfrac{\lambda_u - \lambda_f}{2\Delta T}\left[T - (T_p - \Delta T)\right], & (T_p - \Delta T) \le T \le (T_p + \Delta T), \\ \lambda_u, & T > (T_p + \Delta T), \end{cases} \quad (9)$$

where the subscripts f and u represent the frozen and unfrozen states, respectively; l is the latent heat per unit volume.

3.3. Thermal Parameters and Boundary Conditions. At the elevation of approximately 4500 m on the QTP, the physical parameters for air and crushed-rock layer in the simulations are listed in Table 2. The mean particle size of the CRR is approximately 0.2 m (diameter range from 0.1 to 0.3 m). Thermal parameters needed for the soil layers and embankment fill can be found in Table 3.

To simplify the boundary conditions, the temperature boundaries are employed to the air and ground surfaces. Based on the "adherent layer theory," simplified thermal boundaries are given in equation (10) and Table 4. The geothermal heat flux at the bottom boundaries was assumed to be 0.06 W/m^2. The lateral boundaries were assumed to be adiabatic:

$$T = T_0 + A \sin\left(\frac{2\pi}{8760} t_h + \frac{\pi}{2}\right) + \frac{\Delta T}{365 \times 24} t_h, \quad (10)$$

where T_0 is the annual average value, A is the amplitude, t_h is the time, and ΔT is air temperature rising rate, which is taken as 0.052°C/year on the QTP [26, 30].

The ambient wind affects the convection process in the rock layer. The wind boundary is applied at one side of the model to simulate the prevailing wind direction of north and northwest on the QTP. Based on the observed data for wind on the QTP, wind speed v_h at the height of h in prevailing north direction can be obtained as

$$v_h = \left(4.6 + 1.52 \sin\left(\frac{2\pi}{365 \times 24} t + \frac{3\pi}{2}\right)\right)\left(\frac{h}{10}\right)^{0.16}. \quad (11)$$

3.4. Model Validation. To verify the numerical model, we simulated the thermal regime of a CRR embankment built on Huashixia of the QTP. The simulated and observed temperature profiles at the shady shoulder of the embankment in 2014, one year after construction are shown in Figure 7. It illustrates that the computed temperature curve can fit well with the measured results for the permafrost layer. A large difference between the measurement and simulation was found for the active layer, which mainly results from the simplified boundaries and geological conditions in the model. In general, the numerical model is reasonable for simulating the thermal regime of a crushed-rock embankment in a permafrost region.

4. Numerical Results and Analyses

4.1. Predicted Temperature Fields. Three cases over a 30-year period were simulated. Firstly, the thermal regimes of embankment with CRR when maximum thawing depth reaches in the 5th and 10th years after construction are shown in Figure 8. It can be seen that the temperature field of the CRR embankment is basically symmetrical after construction and the permafrost table under the embankment elevates to near the original ground surface. Such characteristics are similar to the monitored embankment (Figure 3). The CRR begins to show the cooling effect on the permafrost beneath the embankment slopes in the 5th year and beneath the embankment in the 10th year, as indicated by the cold temperature zone of −1.0°C, which gradually expands, as shown in Figure 8. Figure 9 gives thermal regimes of embankment in three cases when maximum thawing depth reaches in the 15th year after construction. The cooling effect of the CRR weakens under the impact of climate warming, as indicated by the shrink of the −1.0°C and −0.8°C isotherms (Figure 9(a)). However, if the rock layer near the toes begins to be filled with sands after the 10th service year (Case 2), the cooling of the CRR will be further weakened, causing obvious warming of the underlying permafrost, as indicated by the rapid shrink of −0.8°C isotherm in Figure 9(b).

In contrast, if the CRR is reinforced by the NMS in the 10th service year, the cooling of the embankment will be improved significantly (Case 3). As shown in Figure 9(c), the colder regions of −1.5°C and even −1.8°C form under the embankment and the permafrost table beneath the embankment slopes is also further elevated obviously after five years' reinforcement. All of these demonstrate the good cooling performance of the new design.

Figure 10 reveals the thermal regimes of embankment in three cases when maximum thawing depth reaches in the 20th year after construction. As shown in Figure 10(a), the disappearance of −1.0°C beneath the embankment indicates that the permafrost temperature obviously increases due to

Table 2: Physical parameters of air and crushed-rock layer [24, 28, 29].

Physical parameters	C (J·m^{-3}·°C^{-1})	λ (W·m^{-1}·°C^{-1})	P (kg·m^{-3})	μ (kg·m^{-1}·s^{-1})	K (m^2)	B (m^{-1})
Air	0.644×10^3	0.02	0.641	1.75×10^{-5}	—	—
Rock layer	1.016×10^6	0.442	—	—	1.39×10^{-5}	211.2

Table 3: Thermal parameters of different media [24, 26, 30].

Thermal parameters	C_{fs} (J·m^{-3}·°C^{-1})	λ_{fs} (W·m^{-1}·°C^{-1})	C_{us} (J·m^{-3}·°C^{-1})	λ_{us} (J·m^{-3}·°C^{-1})	l (J·m^{-3})
Embankment fill	1.913×10^6	1.980	2.232×10^6	1.919	2.01×10^7
Sand	1.465×10^6	0.258	1.465×10^6	0.258	0
Gravel soil	1.863×10^6	2.610	2.401×10^6	1.910	2.32×10^7
Weathered stone	2.122×10^6	1.824	2.413×10^6	1.474	3.81×10^7
Ballast	1.006×10^6	0.346	1.006×10^6	0.346	0

Table 4: Temperature parameters in Equation (10).

Boundaries	T_0 (°C)	A (°C)
Air	−3.8	11.5
Natural ground surfaces	−0.6	12.0
Top surface	0.3	14.0
Crushed-rock surface	1.4	15.2
Embankment slope surfaces	0.8	13.0
Sand surface	0.6	14.0

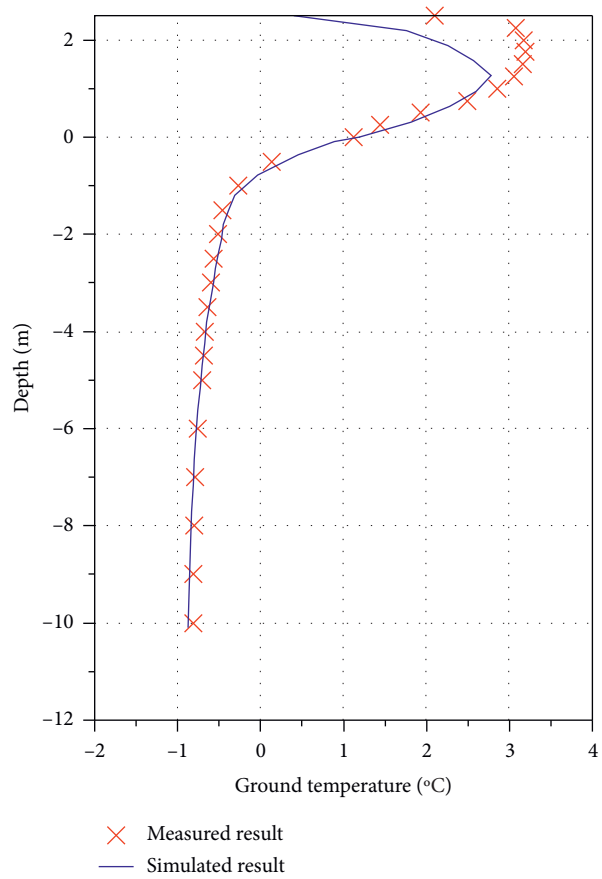

Figure 7: Comparison of the measured and simulated ground temperatures of a CRR embankment on October 15.

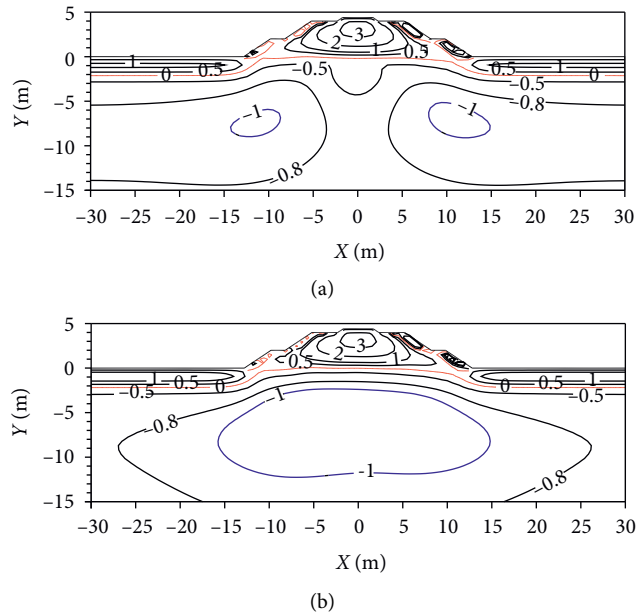

Figure 8: Thermal regimes of embankment with CRR when maximum thawing depth reaches in the 5th (a) and 10th (b) years after construction.

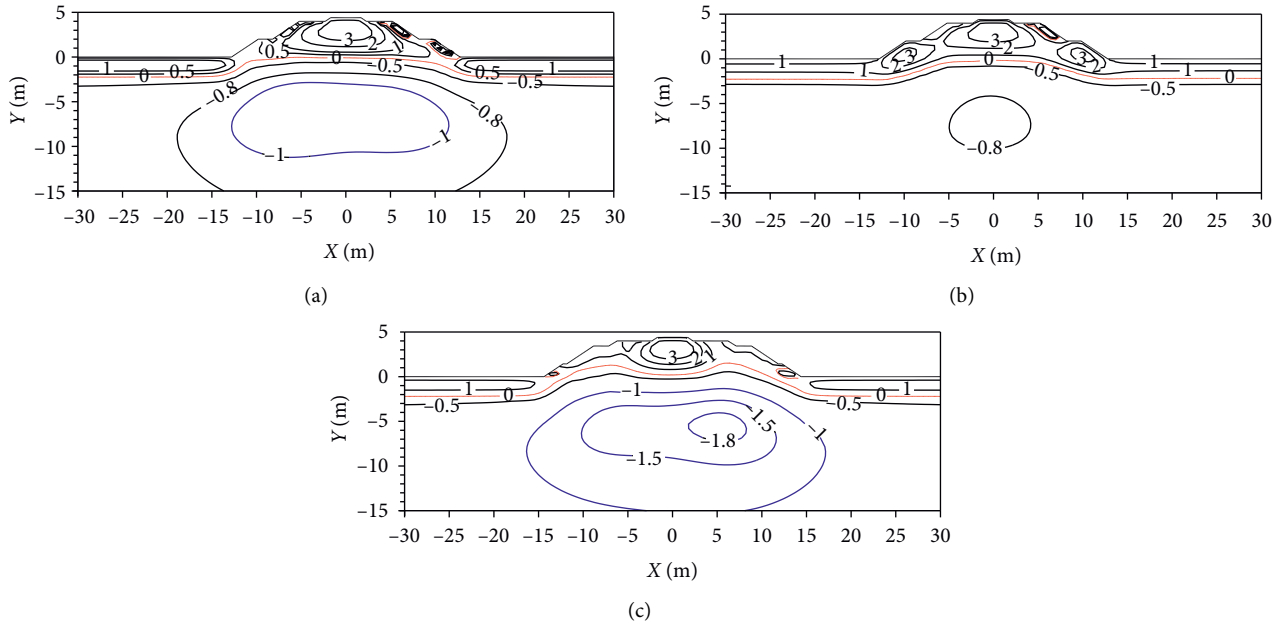

Figure 9: Thermal regimes of embankment in three cases when maximum thawing depth reaches in the 15th year after construction. (a) CRR embankment; (b) CRR filled with sands; and (c) CRR reinforced with NMS.

the weak cooling of the CRR structure. Warm permafrost (>−1.0°C) is generated beneath the embankment and may cause instability in the embankment because the deformation of the permafrost is promoted by the increase in temperature. For Case 2 (Figure 10(b)), sand-filling seriously affects the convection cooling of the rock layer, leading to severe permafrost warming beneath the embankment, particularly under the embankment slopes, indicated by the downward of −0.5°C while for the embankment reinforced by the NMS (Figure 10(c)), the −1.0°C and −1.5°C isotherms still exist under the embankment, revealing the cold thermal state of the permafrost.

As shown in Figure 11(a), in the 30th year after construction, the permafrost temperature beneath the CRR obviously increases because of climate warming. This implies that the sole CRR cannot produce strong enough cooling for the underlying permafrost to maintain the foundation stability. The sand-filling causes not only the permafrost

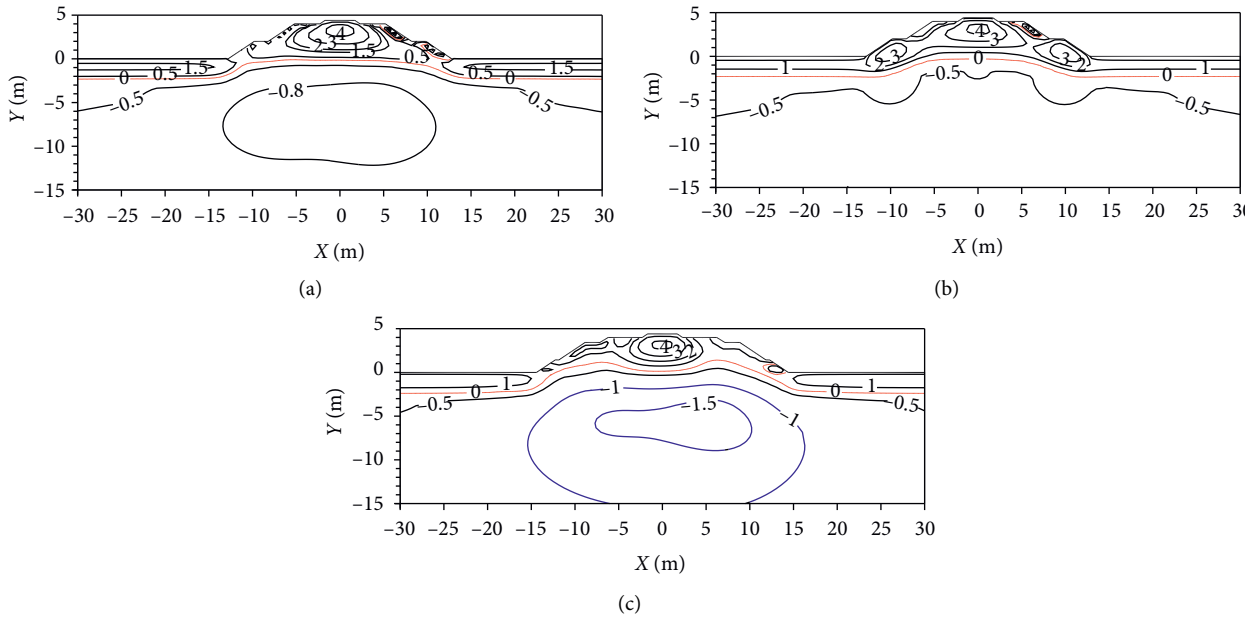

Figure 10: Thermal regimes of embankment in three cases when maximum thawing depth reaches in the 20th year after construction. (a) CRR embankment; (b) CRR filled with sands; and (c) CRR reinforced with NMS.

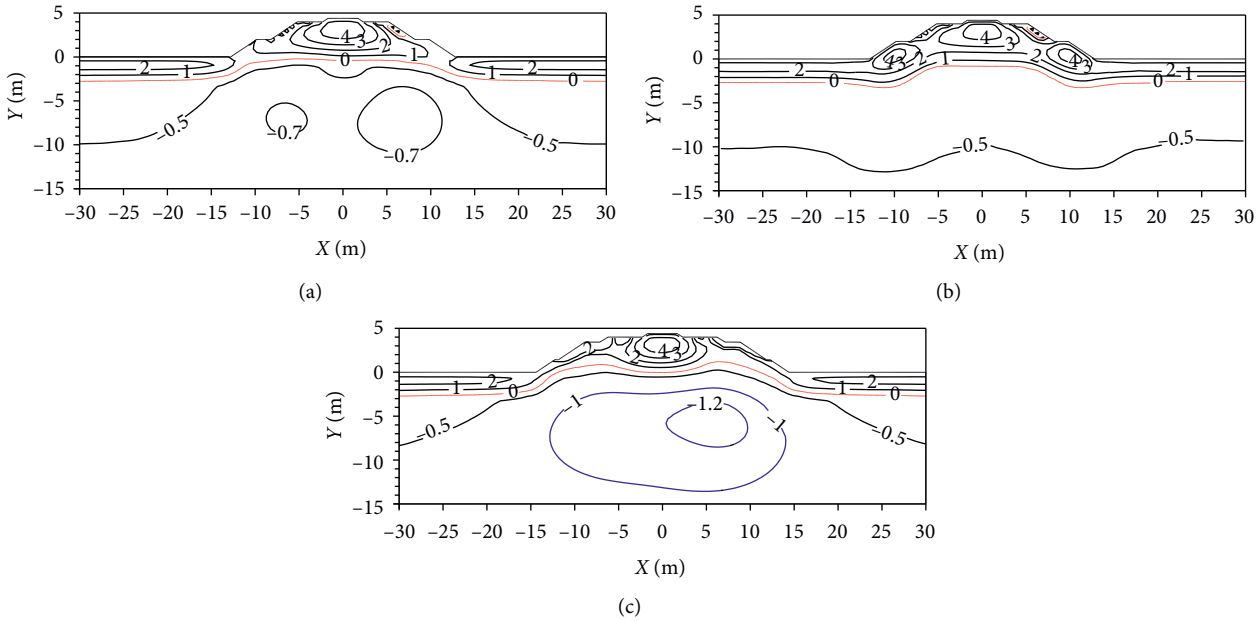

Figure 11: Thermal regimes of embankment in three cases when maximum thawing depth reaches in the 30th year after construction. (a) CRR embankment; (b) CRR filled with sands; and (c) CRR reinforced with NMS.

warming but also the severe permafrost thawing under the slope toes, as indicated by the obvious decline of the permafrost table, as shown in Figure 11(b). Such a process might lead to structure failure of the embankment. The most noticeable characteristic for the new design is the cold zone of −1.0°C, as shown in Figure 11(c), which still covers most regions beneath the embankment to ensure its thermal stability under climate warming. Meanwhile, the permafrost table especially under the embankment slopes rises further into the embankment body, revealing the permafrost aggradation under the effective and sufficient cooling of the NMS.

4.2. Predicted Long-Term Ground Temperature Variations. Figure 12 shows variations of the annual average ground temperatures at a depth of 15 m relative to the original ground surface beneath the centerline of the embankment in

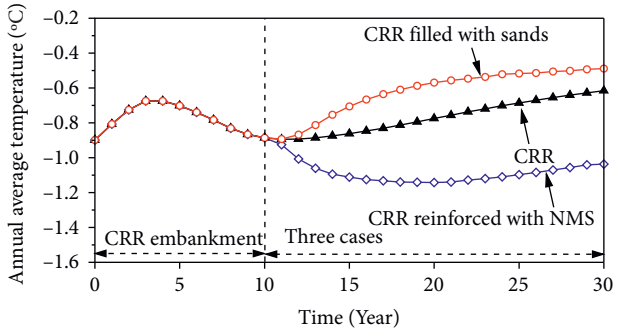

Figure 12: Variations of annual average ground temperatures at 15 m deep underneath the centerline of embankment in three cases during 30 service years.

three cases. It can be found that three stages including thermal disturbance stage, cooling process, and warming process occur in the studied cases. As shown, permafrost at the 15 m depth beneath the CRR experiences a short period of cooling before the 10th year and then experiences a steady warming trend, resulting in nearly 0.3°C temperature rising in the 30th year. The sand-filling can further weaken the convection cooling of the porous rock layer and causes rapid permafrost warming of the foundation. In contrast, the cooling of the NMS can significantly decrease the foundation temperatures and causes obviously decreased temperature than the CRR, which reveals a significant influence on the thermal status of the underlying permafrost of the new structure. Reinforced by the new structure, the permafrost temperature at the depth of 15 m beneath the centerline obviously decreases and is lower than that under the CRR, with a difference of nearly 0.4°C in the service year. It demonstrates the superior cooling effect of the new design and its good reinforced cooling performance.

The new mitigation also plays a role in sand-filling prevention. Although the sand may clog the slope toe and then decrease forced convection cooling, most of the other porous regions exist. Even if the toe is blocked with time, it is not difficult to clean the sand in this small area. A layer of hollow concrete brick with large pore space or a sand-controlling net fence could be arranged close to the slope toe of the new mitigation for further sand prevention.

5. Conclusions

In this study, a traditional CRR embankment over warm permafrost was selected to investigate its cooling characteristics based on the long-term ground temperature observations. An optimized structure was designed to improve the cooling capacity of the CRR and to counter the pore-filling of the rock layer. Numerical simulations were conducted to evaluate the cooling performance and reinforcing capacity of the new structure in sandy permafrost zones based on a developed heat and mass transfer model. The following conclusions can be drawn:

(1) The field results revealed that the traditional CRR could improve the symmetry of the ground temperature distribution, elevate the permafrost table, and decrease the ground temperature of shallow permafrost. However, the cooling capacity of this structure was limited and it could not generate strong enough cooling to influence the deep warm permafrost, causing slow but steady warming of deep permafrost after construction.

(2) The simulated results indicate that the CRR generates an insufficient cooling effect on the warm permafrost and thus cannot maintain the thermal stability of embankment built on warm and thaw-sensitive permafrost under climate warming. The wind-blown sand can further weaken the cooling of the CRR and cause significant permafrost warming and thawing beneath the slopes, posing a severe threat to the long-term safe operation of the embankment.

(3) The NMS can produce a significantly superior cooling performance to the CRR. If the CRR is reinforced by the new structure, it can not only effectively cool the underlying warm permafrost but also elevate the permafrost table. The new structure can also protect the rock layer on the slopes from sand-filling. Therefore, the NMS can be used as an effective method for roadbed design or maintenance over warm permafrost.

Data Availability

The data used to support the findings of this study are included within the article.

Conflicts of Interest

The authors declare that they have no conflicts of interest.

Acknowledgments

This research was supported by the National Key R&D Program of China (Grant no. 2018YFC1505001), the National Natural Science Foundation of China (Grant no. 41701067), the West Light Foundation of Chinese Academy of Sciences (Granted to Dr. Minghao Liu), and the Program of the State Key Laboratory of Frozen Soil Engineering (Grant no. SKLFSE-ZQ-48).

References

[1] R. van Everdingen, *Multi-Language Glossary of Permafrost and Related Ground-Ice Terms*, World Data Center for Glaciology, Boulder, CO, USA, 1998.

[2] Permafrost Subcommittee, *Glossary of Permafrost and Related Ground-Ice Terms*, Associate Committee on Geotechnical Research, National Research Council of Canada, Ottawa, Canada, 1988.

[3] S. Gruber, "Derivation and analysis of a high-resolution estimate of global permafrost zonation," *The Cryosphere*, vol. 6, no. 1, pp. 221–233, 2012.

[4] F. E. Nelson, "Geocryology: enhanced: (un) frozen in time," *Science*, vol. 299, no. 5613, pp. 1673–1675, 2003.

[5] F. E. Nelson, O. A. Anisimov, and N. I. Shiklomanov, "Subsidence risk from thawing permafrost," *Nature*, vol. 410, no. 6831, pp. 889-890, 2001.

[6] G. Cheng, "A roadbed cooling approach for the construction of Qinghai-Tibet railway," *Cold Regions Science and Technology*, vol. 42, no. 2, pp. 169–176, 2005.

[7] M. C. Alfaro, G. A. Ciro, K. J. Thiessen, and T. Ng, "Case study of degrading permafrost beneath a road embankment," *Journal of Cold Regions Engineering*, vol. 23, no. 3, pp. 93–111, 2009.

[8] H.-j. Jin, Q.-h. Yu, S.-l. Wang, and L.-z. Lü, "Changes in permafrost environments along the Qinghai-Tibet engineering corridor induced by anthropogenic activities and climate warming," *Cold Regions Science and Technology*, vol. 53, no. 3, pp. 317–333, 2008.

[9] R. Fortier, A.-M. LeBlanc, and W. Yu, "Impacts of permafrost degradation on a road embankment at Umiujaq in Nunavik (Quebec), Canada," *Canadian Geotechnical Journal*, vol. 48, no. 5, pp. 720–740, 2011.

[10] B. Wang and H. M. French, "Permafrost on the Tibet Plateau, China," *Quaternary Science Reviews*, vol. 14, no. 3, pp. 255–274, 1995.

[11] G. D. Cheng, "Some difference of permafrost on the Qinghai-Tibet Plateau of China and northern Canada," *Journal of Glaciology and Geocryology*, vol. 2, no. 1, pp. 39–42, 1980.

[12] G. Doré, F. Niu, and H. Brooks, "Adaptation methods for transportation infrastructure built on degrading permafrost," *Permafrost and Periglacial Processes*, vol. 27, no. 4, pp. 352–364, 2016.

[13] Q. B. Wu, S. Y. Zhao, W. Ma, Y. Z. Liu, and L. X. Zhang, "Monitoring and analysis of cooling effect of block-stone embankment for Qinghai-Tibet railway," *Chinese Journal of Geotechnical Engineering*, vol. 27, pp. 1386–1390, 2005.

[14] D. J. Goering and P. Kumar, "Winter-time convection in open-graded embankments," *Cold Regions Science and Technology*, vol. 24, no. 1, pp. 57–74, 1996.

[15] Q. B. Wu, H. T. Zhao, Z. Q. Zhang, J. Chen, and Y. Z. Liu, "Long-term role of cooling the underlying permafrost of the crushed rock structure embankment along the Qinghai-Xizang railway," *Permafrost and Periglacial Processes*, vol. 31, no. 4, pp. 172–183, 2019.

[16] Y. M. Lai, M. Y. Zhang, and S. Y. Li, *Theory and Application of Cold Regions Engineering*, Science Press, Beijing, China, 2009.

[17] Y. Mu, W. Ma, Y. Liu, and Z. Sun, "Monitoring investigation on thermal stability of air-convection crushed-rock embankment," *Cold Regions Science and Technology*, vol. 62, pp. 160–172, 2010.

[18] W. Ma, Q. B. Wu, and G. D. Cheng, "Analyses of the temperature fields within an air convective embankment of crushed rock structure along the Qinghai-Tibet railway," *Journal of Glaciology and Geocryology*, vol. 28, no. 4, pp. 586–594, 2006.

[19] L. Chen, W. Yu, F. Han, Y. Lu, and T. Zhang, "Effects of desertification on permafrost environment in Qinghai-Tibetan Plateau," *Journal of Environmental Management*, vol. 262, Article ID 110302, 2020.

[20] Z. J. Lin, F. J. Niu, H. Liu, and J. H. Lu, "Influences of freezing-thawing cycles on physico-mechanical properties of rocks of embankment revetments in permafrost regions," *Rock and Soil Mechanics*, vol. 32, no. 5, pp. 1369–1376, 2011.

[21] M. T. Chai, Y. H. Mu, J. M. Zhang, W. Ma, G. Liu, and J. B. Chen, "Characteristics of asphalt pavement damage in degrading permafrost regions: case study of the Qinghai-Tibet highway, China," *Journal of Cold Regions Engineering*, vol. 32, no. 2, pp. 5–18, 2018.

[22] W. Ma, Y. Mu, Q. Wu, Z. Sun, and Y. Liu, "Characteristics and mechanisms of embankment deformation along the Qinghai-Tibet railway in permafrost regions," *Cold Regions Science and Technology*, vol. 67, no. 3, pp. 178–186, 2011.

[23] J. L. Qi, Y. Sheng, J. M. Zhang, and Z. Wen, "Settlement of embankments in permafrost regions in the Qinghai-Tibet plateau," *Norsk Geografisk Tidsskrift-Norwegian J. Geography*, vol. 61, no. 2, pp. 49–55, 2007.

[24] M. Zhang, Y. Lai, F. Niu, and S. He, "A numerical model of the coupled heat transfer for duct-ventilated embankment under wind action in cold regions and its application," *Cold Regions Science and Technology*, vol. 45, no. 2, pp. 103–113, 2006.

[25] W. Q. Tao, *Numerical Heat Transfer*, Xi'an Jiaotong University Press, Xi'an, China, 2004.

[26] Y. M. Lai, L. X. Zhang, S. J. Zhang, and L. Mi, "Cooling effect of ripped-stone embankments on Qinghai-Tibet railway under climatic warming," *Chinese, Science Bullitin*, vol. 48, no. 6, pp. 598–604, 2003.

[27] L. N. Zhu, "Study of the adherent layer on different types of ground in permafrost regions on the Qinghai-Xizang plateau," *Journal of Glaciology and Geocryology*, vol. 10, no. 1, pp. 8–14, 1988.

[28] M. Zhang, Y. Lai, D. Li, W. Chen, and G. Tong, "Experimental study on ventilation characteristics of a concrete-sphere layer and a crushed-rock layer," *International Journal of Heat and Mass Transfer*, vol. 59, pp. 407–413, 2013.

[29] X. Z. Xu, J. C. Wang, and L. X. Zhang, *Physics of Frozen So*, Science Press, Beijing, China, 2001.

[30] D. H. Qin, Y. H. Ding, and S. W. Wang, "A study of environment change and its impacts in western China," *Frontiers in Earth Science*, vol. 9, no. 2, pp. 321–328, 2002.